**[Supplementary material]**

**The metal behind the myths: iron metallurgy in the south-eastern Black Sea region**

Nathaniel L. Erb-Satullo[1,*], Brian J.J. Gilmour[1] & Nana Khakhutaishvili[2]

[1] *School of Archaeology, Oxford University, Oxford, United Kingdom.*

[2] *Department of History, Archaeology and Ethnology, Shota Rustaveli State University, Batumi, Republic of Georgia*

[*] *Author for correspondence (Email: nathaniel.erb-satullo@arch.ox.ac.uk)*

**Survey of metallurgical sites**

Survey of metallurgical sites in western Georgia posed a number of methodological challenges. Because the methods of systematic survey were wholly unsuitable for these hilly, densely-vegetated landscapes, survey relied upon unpublished Soviet-period field notebooks and local informants. The table below (Table S1) provides further detail on the spatial position and character of metallurgical sites identified on survey. Sites were characterised by a concentration of metallurgical debris, primarily slag but also including tuyères, furnace fragments, and sometimes discarded ore fragments. Non-technical ceramics (i.e. ceramic material other than clay furnace fragments and tuyères), which might have provided diagnostic chronological information, were rare. Because of heavy vegetation in these landscapes, most sites were identified because they had been encountered during modern road-building or agricultural activities. As a result, preservation and surface exposure was variable. The type of metal produced at these sites was identified by a combination of macroscopic examination, qualitative portable X-ray fluorescence (pXRF) analysis (to check for the presence or absence of diagnostic metal elements), and intensive optical microscopy and SEM-EDS analysis.

**Table S1. Metallurgical sites identified in mountainous Adjara and Samegrelo areas. Coordinates are given in UTM Grid 38N. Note that sites 1–56 are copper-smelting sites found by the project in other areas of western Georgia and published elsewhere (see Erb-Satullo et al. 2017).**

| Site # | Site name | Easting | Northing | Site type | Site description |
|---|---|---|---|---|---|
| 57 | Tago I | 275754 | 4610779 | Iron-smelting site | Disturbed site in garden plot behind a house. Poor visibility and exposure. |
| 58 | Tago II | 275688 | 4610644 | Iron-smelting site | Slag scatter spread over gently sloping ground with short grass and maize field. |
| 59 | Dzmagula I | 274353 | 4609024 | Iron-smelting site | Slag heap on very steeply sloping ground, cut by road construction. Large exposed section of slag heap visible. Rest of site probably covered by landslides. |
| 60 | Chao I | 274405 | 4610996 | Iron-smelting site | Heap of tap and furnace slag, probably disturbed by land clearance for small agricultural fields. |
| 61 | Cheri I | 276035 | 4607972 | Iron-smelting site | Tap and furnace slag in road cut near cemetery. |
| 62 | Gurdzauli I | 276718 | 4609203 | Iron mining site (?) | Possible debris heap from mining in stream bed. Iron-rich water in stream has stained downstream rocks red. A single small piece of slag was found in the adjacent roadway. |
| 63 | Dzmagula II | 274337 | 4609248 | Iron-smelting site | Scatter of slag (highly disturbed) in garden plot. Large pieces were collected by farmers and piled on the upslope edge of the field. |
| 64 | Tsablana I | 280144 | 4607897 | Iron-smelting site | Dense accumulation of slag at bottom of very steep west-facing hillslope. In field above, a slight bulge in the slope is visible, indicating the probable extent of the slag heap. Tap slag predominates in the artefacts visible at the surface. |

| 65 | Tsablana II | 279970 | 4607240 | Iron-smelting site | Highly disturbed smelting site in maize field, with cairn of slag produced by recent agricultural clearance. Small fragment of obsidian found nearby. |
|----|-------------|--------|---------|---------|---------|
| 66 | Cheri II | 276218 | 4608054 | Iron mining and smelting site | Large slag heap on steeply sloping ground. Nearby landslip has partially eroded the slag heap, but the remainder seems relatively undisturbed. Above the slag heap, small mining galleries were identified, which cut into the exposed rock outcrop. |
| 67 | Kinchauri I | 277895 | 4606339 | Iron-smelting site | Large scatter of slag in agricultural field. Tap and furnace slags as well as technical ceramics and possible ore. Undisturbed slag heap not identified. |
| 68 | Dzmagula III | 275001 | 4609298 | Iron-smelting site | Scatter of slag (mostly dense with one possible piece of tap slag) in agricultural fields. Deposits probably disturbed. |
| 69 | Pachkha I | 278436 | 4609322 | Iron-smelting site | Disturbed slag deposits in agricultural fields and roadways on south-southeast facing hillside. |
| 70 | Pachkha II | 278327 | 4609325 | Iron-smelting site | Disturbed scatter of slag found on either side of road and (according to local villagers) in neighbouring maize field. |
| 71 | Pachkha III | 277702 | 4609087 | Iron-smelting site | Well preserved slag heap on S facing slope in woodland. |
| 72 | Tsablana III | 279141 | 4606910 | Iron-smelting site | Smelting site partially damaged by road building. Slag scattered downhill from road cut. |
| 73 | Cheri III | 275621 | 4608165 | Iron-smelting site | Pieces of slag found in roadway. Pieces are small enough and scarce enough that it is possible they come from higher up on the slope. Further investigation needed. |

| 74 | Chogha I | 270751 | 4716817 | Copper-smelting site | Previously excavated site dated to the first half of the first millennium BC with both spongy and dense slag cake fragments. Site located in overgrown tea plantation, but a pile of slag 3–4m in diameter (probably piled up in process of excavation) is clear of vegetation. See Khakhutaishvili (2009: 95–104) for more details. |
|----|----------|--------|---------|----------|---------|
| 75 | Chogha II | 271016 | 4716981 | Copper-smelting site | Previously excavated site dated to the first half of the first millennium BC in dense vegetation of an overgrown tea plantation. Spongy and dense slags present, along with technical ceramic. See Khakhutaishvili (2009: 95–104) for more details. |
| 76 | Uncertain | 268939 | 4716065 | Metal production and possible settlement | Small pieces of pottery, slag and flecks of charcoal exposed in road cut by Ochkhomuri River. Unclear whether this is an in-situ deposit or hillwash from a site farther up the slope. Site 76 and Site 77 might be part of the same settlement complex. Khakhutaishvili (2009: 95) mentions an unexcavated Iron Age settlement somewhere close by; sites 76 and 77 may part of that site. |
| 77 | Uncertain | 269082 | 4716118 | Iron production (smithing?) and possible settlement | Several pieces of slag (one potential smithing hearth bottom) and a tuyère found on slopes. Probably material eroded from densely vegetated area higher up on the slope. Local villagers reported finding ceramics when planting hazelnut trees in the vicinity. Site 77 and Site 76 may be part of the same general complex. Khakhutaishvili (2009: 95) mentions an unexcavated Iron Age |

| | | | | | settlement somewhere close by; sites 76 and 77 may be part of that site. |
|---|---|---|---|---|---|
| 78 | Zumi I | 266349 | 4720875 | Iron-smelting near settlement | Iron-smelting slag scattered in a maize field. Highly disturbed but probably part of the larger settlement and smelting complex along with Zumi II. Tap slag is very glassy. |
| 79 | Nakiani I | 269674 | 4711512 | Iron-smelting and settlement | Light scatter of metallurgical remains on hillslope below a terraced area and mound on hilltop. Mound is similar to that found at Site 81, but its purpose is unclear. |
| 80 | Jumiti I | 264413 | 4714499 | Iron-smelting site | Significant scatter of slag on sloping ground above Khobi River. |
| 81 | Napichkhovo I | 271618 | 4719981 | Iron-smelting and settlement | Diffuse scatter of slag over large area over cultivated and grazing land. Smelting activities are clearly part of a larger complex, with levelled terraces, a hilltop mound, and ditch cut into bedrock. Possible evidence of collapsed stone architecture, but very poor ground visibility made it difficult to assign a date. A possible fragment of mortared masonry was identified. |
| 82 | Naukhramu I | 274643 | 4721730 | Iron-smelting site with other structures | Thinly scattered slag in dense forested area with evidence of stone architecture. Surface visibility extremely poor and dating of these features is unclear. |
| 83 | Zumi II | 266229 | 4720846 | Iron-smelting and settlement | Substantial quantities of slag (often with quite glassy appearance) spread over a large area. Probably part of the same complex as Site 78—they are quite close. Much slag is glassy, and tuyère fragments were identified. Above the slag scatter, there are a number of terraces, with some evidence of stone architecture. A few small fragments of coarse unidentified |

| | | | | | ceramics were found here. Evidence for settlement is spread over several adjacent rises above the smelting remains of Sites 78 and 83. |
|---|---|---|---|---|---|
| 84 | Jumiti II | 263541 | 4713560 | Iron-smelting with possible smithing | Large low-density scatter of slag probably disturbed by ploughing for agricultural activities. Finds include some possible smithing hearth bottoms and tap slags. |

Traces of ancient activities besides smelting was identified near several smelting sites (Figure S1). Several examples of possible smithing hearth bottoms were noted (e.g. at Sites 84 and 77, see Tables S1 & S3). Unequivocal mining activities were identified at Site 66 adjacent to the slag heap, and a possible mining area was identified farther up the same ravine at Site 62. Smelting debris at a number of sites in Samegrelo was discovered in association with larger complexes including linear stone features, terraces, and mounds. Often the smelting debris would be found on the margins of these complexes, situated on lower slopes. Thick grassy turf and other vegetation precluded surface collection of ceramics to accurately date these remains. Nevertheless, it is noteworthy that the spatial association of smelting remains with larger complexes of walls, terraces, and mounds was observed at a number of Samegrelo sites (78, 79, 81, 82 & 83), the last of which was dated by slag-encased charcoal to the mid- to late-first millennium BC. Nothing similar has been recorded at earlier Late Bronze to Early Iron Age copper-smelting sites, or at medieval iron-smelting sites in Adjara. Naturally, more intensive investigation at these sites would be necessary to pin down the chronological development of these complexes, but it is conceivable that they reflect a spatial organization of iron metallurgy that is specific to the mid- to late-first millennium BC.
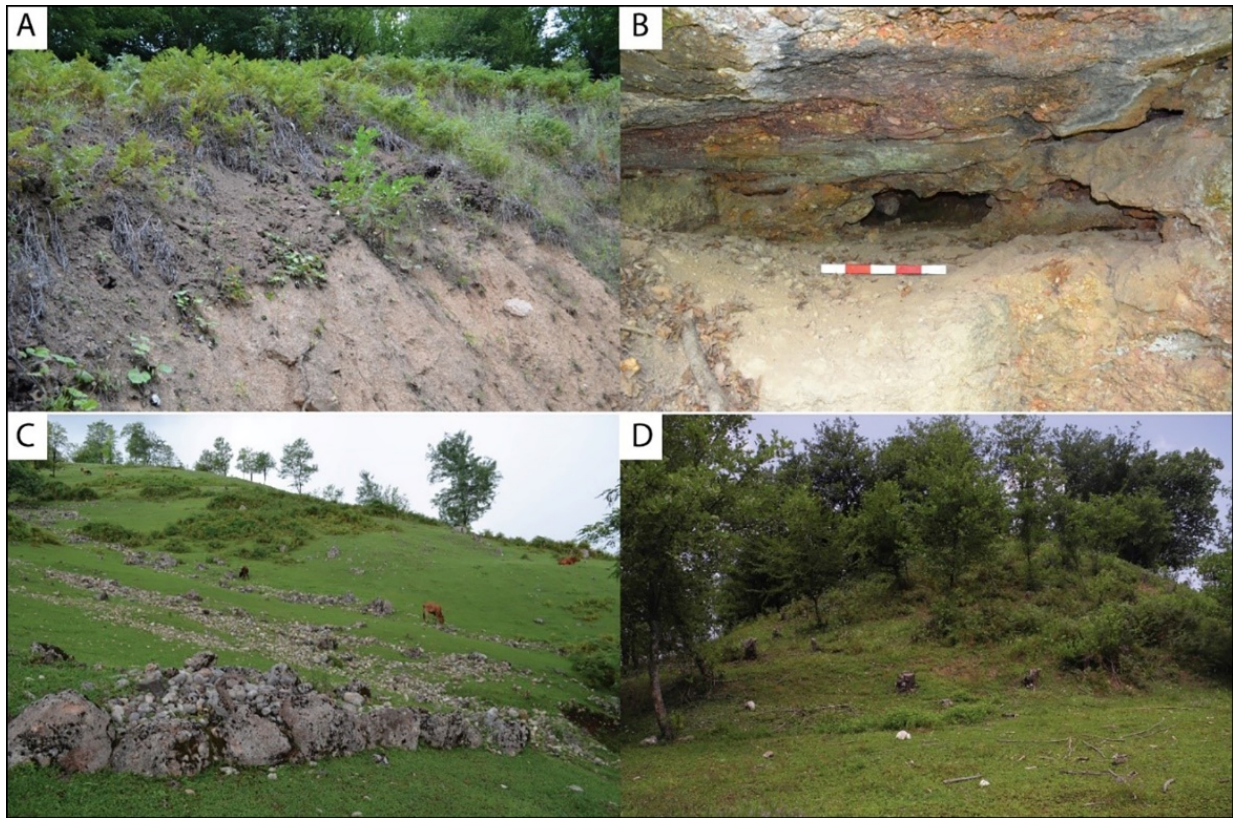
*Figure S1. Slag heaps and other features identified on survey: A) Eroded portion of slag heap (dark grey deposit) at Site 66. Mining activity shown in (B) was found at the tree-line in the background; B) traces of ancient mining activity at Site 66. Scale bar is 0.5m; C) linear stone features on hill above smelting sites 83 and 78; D) anthropogenic mound on hill above smelting debris at Site 79.*

**Table S2. Table of radiocarbon dates from iron-smelting sites. Dates from Erb-Satullo *et al*. (2018: 174).**

| Site # | Field # | Lab # | Material | Uncalibrated Date (radiocarbon yrs BP) | Calibrated date range (2σ) |
|---|---|---|---|---|---|
| 59 | RC-13-18 | OxA-30108 | *Fagus sylvatica; Corylus; Castanea/Quercus* wood charcoal | 766±23 | AD 1222–1280 |
| 59 | RC-13-19a | OxA-30109 | *Juglans regia* wood charcoal | 777±23 | AD 1220–1276 |

| 59 | RC-13-19b | OxA-30110 | *Juglans regia* wood charcoal | 817±24 | AD 1170–1264 |
|---|---|---|---|---|---|
| 64 | RC-13-32 | OxA-30111 | *Carpinus* wood charcoal | 860±23 | AD 1054–1079 (4.6%); AD 1152–1246 (90.8%) |
| 66 | RC-13-25 | OxA-30112 | *Quercus* wood charcoal | 666±23 | AD 1278–1315 (51.6%); AD 1355–1389 (43.8%) |
| 80 | RC-14-31 | AA105846 | Angiosperm wood charcoal | 2349±32 | 516–370 BC |
| 80 | RC-15-5 | AA107059 | Angiosperm wood charcoal | 2266±40 | 401–346 BC (38.9%); 321–206 BC (56.5%) |
| 83 | RC-14-32 | AA105845 | Angiosperm wood charcoal | 2251±32 | 396–346 BC (31.7%); 321–206 BC (63.7%) |
| 83 | RC-15-8 | AA107058 | Angiosperm wood charcoal (probably *Quercus*) | 2300±27 | 406–357 BC (84.2%); 285–235 BC (11.2%) |
| 84 | RC-14-33 | AA105844 | Angiosperm wood charcoal | 947±30 | AD 1025–1155 |

## Radiocarbon dating of sites

Dating metallurgical sites identified on survey was of paramount concern. Diagnostic non-metallurgical ceramics were rarely found on these sites. Radiocarbon dating of charcoal, either from exposed sections or encased within surface collected slags, proved an effective dating strategy. While direct comparison of slag-heap charcoal and slag-encased charcoal from the same site was not possible, the Classical-Hellenistic dates on charcoal from inside surface-collected slags (4 dates on charcoal from 3 slag fragments on two sites) were consistent within and between sites, strengthening the case for their reliability. There was also no evidence for significant carbonate additions (e.g. $CaCO_3$ or $FeCO_3$) into the furnace charge that might have introduced erroneously old carbon. Detailed discussion of the radiocarbon dates on iron-smelting remains has been reported in another publication (Erb-Satullo *et al.* 2018), but a table of iron-

smelting dates is included here (Table S2). However, additional Bayesian modelling of the dates on charcoal recovered from stratified deposits from Site 59 was undertaken for this paper, as it illustrated the rate of deposition in the slag heap and carried implications for seasonality in iron production in mountainous Adjara. Incorporation of stratigraphic information into the priors using OxCal showed that periods of abandonment were quite short. Samples were taken from contexts 1002 and 1005, which were part of two distinct phases of metallurgical activity at the site separated by a layer of slag-poor sediment 0.2–0.4m thick. We hypothesised that these layers were deposited in relatively quick succession, and the layer of slag-poor sediment may have been fill from digging out the furnace and flat workspace on what was otherwise steeply sloping ground. Radiocarbon dating confirmed that the interval between phases of smelting was quite short. Bayesian modelling of three dates (OxA-30108, OxA-30109 and OxA-30110) suggests that the length of time between the deposition of contexts 1005 and 1002 (which included deposition of a slag-poor buff-coloured sediment, 1003 in between the slag-rich deposits) was between 0 and 32 years (95.4 per cent confidence). The probability density curve (Figure S2) is positively skewed with a maximum at about 2 years, meaning that the interval is far more likely to be less than 16 years than it is to be between 16 and 32 years. These results suggest that smelting took place seasonally, and fairly large amounts of slag were deposited quickly. The picture of seasonal smelting is entirely consistent with the setting of these sites, situated on steep ground in mountain ravines with significant winter snowfall. Accurately assessing the overall scale of production is difficult, as the total volume of the slag heap was impossible to estimate, since colluvial sedimentation and vegetation obscured the parts of the slag heap that were not exposed by the modern road cut.
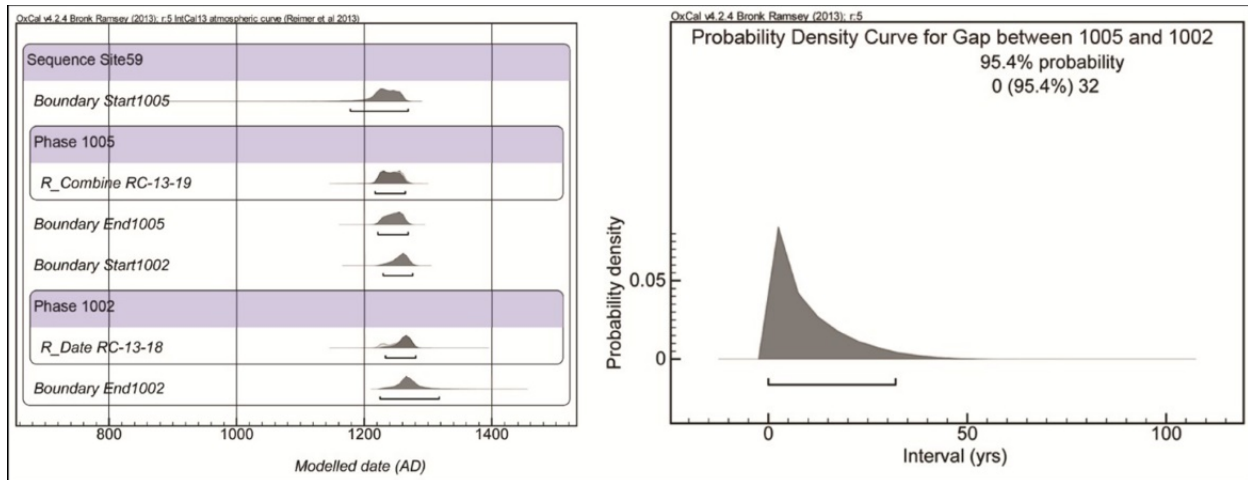
*Figure S2. Bayesian modelling of interval between the deposition of 1005 and 1002. See main article (Figure 3) for a drawing of the stratigraphic section.*

**Further details on the microscopic and chemical analysis of slag samples**

Understanding the chemistry and mineralogy of slag samples was essential for understanding the type of metal produced, the ores used, and the thermodynamic conditions within the furnace. Microscopic associations between different phases, such as the association between iron sulphides and iron oxides/iron metal (Figure S3), can indicate that such materials were added to the charge together. Finds of vitreous (i.e. glassy) or poorly crystallised slags, were a notable feature of both slags from both periods, but were particularly notable at Sites 78 and 83, the latter of which was radiocarbon dated to the Classical/Hellenistic period (Figure S4). Vitreous slags are characterised by the absence (or minimal presence) of crystalline phases (e.g. iron silicates such as fayalite) in the portion of the slag that was once fully molten. Vitreous slags typically have lower iron and more elevated silica content relative to slags with substantial crystalline phases. Occasionally, areas of devitrification, with tiny crystals that are barely resolvable via optical microscopy, are visible in glassy slags, but these are easily distinguished from the formation of larger crystalline phases.
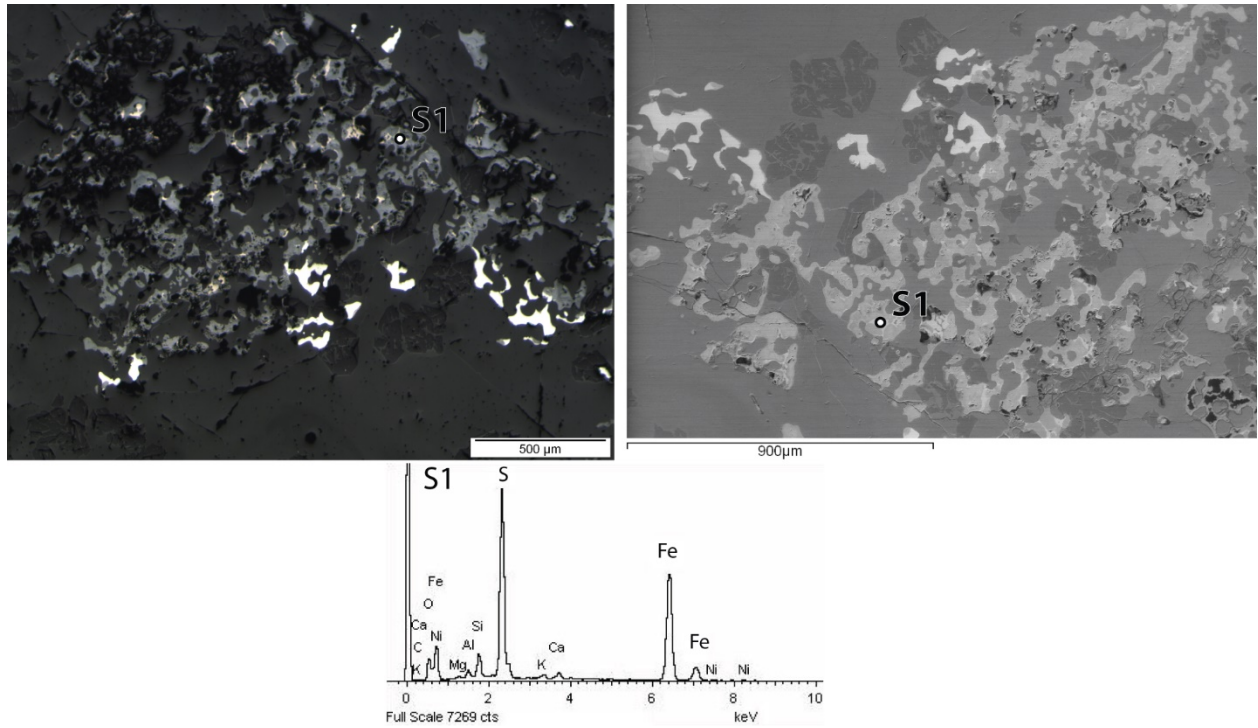
*Figure S3. Optical photomicrograph (left) and scanning electron image (right) of iron sulphides finely intermixed with iron metal and iron oxides in sample 5904, along with an EDS spectrum of the iron sulphide phase.*
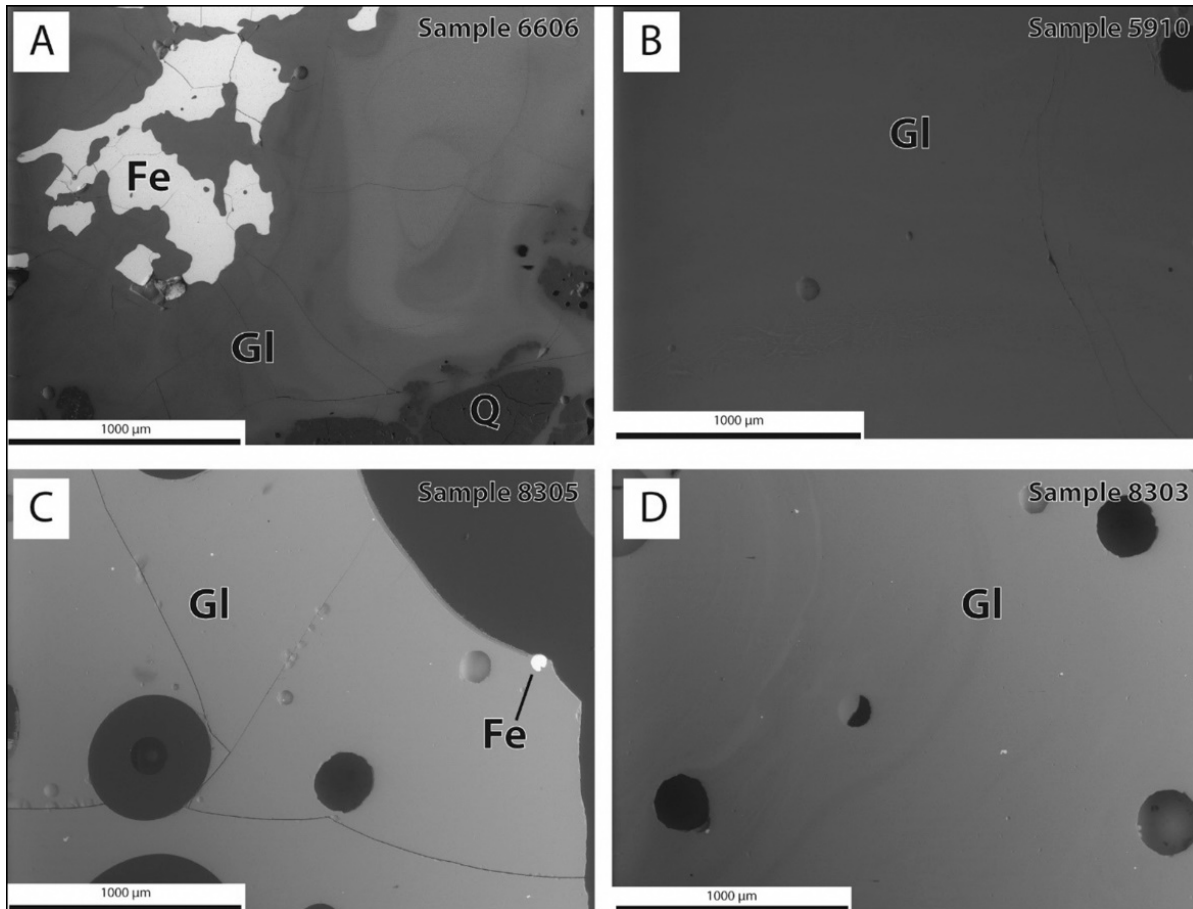
*Figure S4. Examples of microstructures of vitreous slags. Dark circular areas are gas bubbles. Abbreviations: Fe – metallic iron, Q – quartz, Gl – glassy phase.*

Table S3 lists macroscopic slag type, the presence or absence of certain key phases and other features, and a general microscopic description of each sample as determined by optical and scanning electron microscopy. In cases where the presence is loosely quantified, the categories are "present in significant amounts" (XX), "present in a few instances" (X), and "not identified" (—). "Free" iron oxides refer to magnetite and wüstite crystals forming from the melt, which are indicators of the redox conditions at the time of their formation. Not included in this category are iron oxides that formed from the post-depositional corrosion of what was once metallic iron, and hercynite, which is categorised separately. The former is distinguishable based on microstructure and the presence of occasional islands of uncorroded metal. The latter is identifiable due to its low optical reflectance and high aluminium content in SEM-EDS spot analyses. Strictly speaking, in most cases this phase is probably a hercynite-rich solid solution with a composition

between pure hercynite ($FeAl_2O_4$) and pure magnetite ($Fe_3O_4$), which forms a complete solid solution above 850°C (Muralha *et al.* 2011:2081). Relict ore morphologies are clusters of iron oxide or iron metal which preserve textures or shapes that are reflective of the original ore. These structures tend to occur in areas where reduction was either incomplete, or the melt cooled before the reduced metal coalesced into the bloom.

**Table S3. Mineralogy and microstructures of all slags analysed by optical microscopy. Abbreviations: FS – furnace slag (a product of smelting); SHB – smithing hearth bottom (a product of iron smithing); TS – tap slag (a product of smelting); I – indeterminate type (usually for small fragments); XX – present in significant quantities; X – present, but in only a few instances, (—) – not observed. Entries of "none" or "minimal" in the iron oxide form column indicate that iron oxides are absent or virtually absent in the sample.**

| Site # | Sample # | Period | Type | Dominant form of 'free' iron oxides | Metallic iron | Hercynite (Aluminium-rich Spinel) | Relict ore morphologies | Iron sulphides | Iron phosphides | Description |
|---|---|---|---|---|---|---|---|---|---|---|
| 57 | 5701 | Probable medieval | FS | Magnetite/ Wüstite | XX | XX | XX | — | — | Heavily corroded, very heterogeneous slag. Iron oxides are predominantly in relict ore morphologies, but wüstite and magnetite were both observed. Many corroded metallic iron aggregates. |
| 57 | 5702 | Probable medieval | TS | None | XX | XX | — | X | — | Mostly glassy slag with thin iron silicate laths and rounded prills of metallic iron. |
| 58 | 5801 | Probable medieval | FS | Wüstite | XX | XX | X | — | — | Wüstite-rich slag with some leucite, and possible relict ore morphologies. Fairly corroded. |

| 58 | 5802 | Probable medieval | TS | Wüstite | XX | XX | — | — | — | Wüstite and fayalite-dominated slag with some hercynite. |
|----|------|-------------------|----|---------|----|----|----|----|----|----|
| 59 | 5901 | Medieval | FS | Wüstite | XX | X | — | — | — | Large quantities of wüstite along with a number of particles of metallic iron. |
| 59 | 5902 | Medieval | TS | Wüstite/Magnetite | — | XX | — | — | — | Iron silicate laths with tapping bands of iron oxides. Overall little iron oxide; some leucite. Magnetite seen with varying reflectance, SEM-EDS spectra show significant Al presence in some grains. |
| 59 | 5903 | Medieval | FS | Minimal | XX | X | XX | XX | — | Aggregates of metallic iron mimicking ore morphologies, many small prills of iron sulphide. Almost no magnetite/wüstite, small amount of hercynite. Cr/Ti/V detected in Hercynite crystals. Plagioclase feldspars were identified. Some of the plagioclase crystals are growing into the iron aggregates, suggesting the iron was in a liquid state as |

| | | | | | | | | | | |
|---|---|---|---|---|---|---|---|---|---|---|
| | | | | | | | | | | the plagioclase crystals formed. |
| 59 | 5904 | Medieval | FS | Minimal | XX | — | XX | XX | — | Aggregates of metallic iron mimicking ore morphologies. Almost no magnetite/wüstite, significant leucite. |
| 59 | 5906 | Medieval | FS | Minimal | XX | — | — | XX | XX | Sample is essentially a small bloom fragment with adhering glassy slag. Metal has abundant sulphide and phosphide phases. Highly variable microstructure. |
| 59 | 5907 | Medieval | FS | Minimal | XX | XX | XX | XX | — | Fairly corroded slag, with significant metallic iron. Anorthite-rich plagioclase feldspar present. Abundant iron sulphides. Iron oxides present are probably corroded metallic iron. Al-rich and Ti-rich spinels present. |
| 59 | 5910 | Medieval | TS | None | X | — | — | — | — | Glassy slag with one single prill of metallic iron. |
| 59 | 5911 | Medieval | TS | None | X | — | — | — | — | Glassy tap slag with a single tiny iron prill. |
| 59 | 5912 | Medieval | FS | Minimal | XX | — | XX | XX | — | Large aggregates of metallic iron, with textures indicating |

| | | | | | | | | | | |
|---|---|---|---|---|---|---|---|---|---|---|
| | | | | | | | | | | solid-state reduction. Minimal iron oxides, some of which appear to be corroded iron metal. Small prills of iron sulphides. Possible Al-rich spinels (hercynite) in one area near melted technical ceramic. |
| 59 | 5913 | Medieval | TS | Magnetite | — | — | — | — | — | Glassy slag with thin iron silicate laths and rounded prills. Few iron oxides, most of which are concentrated near surface and at tapping bands. Slight more iron oxides than 5914. |
| 59 | 5914 | Medieval | TS | Minimal | X | — | — | — | — | Glassy slag with thin iron silicate laths and rounded prills. A small amount of magnetite is visible at tapping bands. One prill of metallic iron noted. |
| 66 | 6603 | Medieval | FS | None | XX | X | XX | — | — | Large aggregates of metallic iron with leucite in a glassy phase. Minimal iron oxides. (Those present seem to be corroded metallic iron.) |

| 66 | 6604 | Medieval | FS | Wüstite | XX | XX | XX | XX | X | Heterogeneous microstructure: large aggregates of metallic iron, leucite, fine iron oxides, some iron sulphides, possible steadite (iron-iron phosphide eutectic). Leucite was observed, as were some Al-rich spinels (hercynite). |
|---|---|---|---|---|---|---|---|---|---|---|
| 66 | 6605 | Medieval | FS | None | XX | — | XX | XX | — | Abundant iron aggregates, fine silicate crystals, (iron silicates, a feldspar of anorthite-rich composition) and little iron oxides. Some partially reacted quartz. Abundant iron sulphides at the grain boundaries. Phosphide not observed, but it may have been missed (sample not etched). |
| 66 | 6606 | Medieval | FS | None | XX | — | XX | XX | XX | Large aggregates chunks of metallic iron with phosphides (steadite) and sulphides at grain boundaries. Large metal grains characteristic of phosphoric iron. Slag is highly glassy, with no freshly |

| | | | | | | | | | | formed crystalline silicate phases. Some partly reacted quartz. |
|---|---|---|---|---|---|---|---|---|---|---|
| 66 | 6607 | Medieval | TS | Wüstite | — | XX | — | — | — | Wüstite and fayalite-dominated slag with no metallic iron. Tapping bands visible. |
| 66 | 6608 | Medieval | TS | Wüstite | X or XX | XX | — | — | — | Iron silicate laths with interstitial wüstite and small particles of metallic iron. Hercynite present, as well as a small amount of leucite. |
| 66 | 6609 | Medieval | TS | None | — | — | — | XX | — | Thin laths of iron silicate, no iron oxides/metallic iron. Very tiny prills of sulphide in between the fayalite laths. |
| 79 | 7901 | Probable Classical/ Hellenistic | FS | Wüstite | X | XX | — | — | — | Wüstite, fayalite, and hercynite. Wüstite declines closer to adhering technical ceramic. Small particles of metallic iron. |
| 80 | 8004 | Classical/ Hellenistic | FS | None | X | XX | — | XX | — | Sample microstructure varies, in large parts dominated by iron silicates and hercynite. Also present are some equiaxed angular Fe-Ti-Al |

| | | | | | | | | | | |
|---|---|---|---|---|---|---|---|---|---|---|
| | | | | | | | | | | spinels. A single tiny particle of metallic iron. Fine iron sulphide prills present throughout. |
| 80 | 8005 | Classical/ Hellenistic | FS | Minimal | XX | XX | — | XX | — | Fayalite-dominated slag with significant amounts of hercynite but minimal presence of other 'free' iron oxides, which are only observable as minute crystals in between the large fayalite laths. They are too small to identify them as magnetite or wüstite morphologically. Metallic iron is present, but in smaller quantities than some other slags. Corroded metallic iron foils observed in one part of the sample. Very fine sulphide prills are present throughout the sample in the interstices between the fayalite laths. |
| 80 | 8006 | Classical/ Hellenistic | TS | None | X | XX | — | — | — | Slag dominated by iron silicate (probably fayalite) phases and hercynite. In places, the rims of the |

| | | | | | | | | | | hercynite seem to be converting to another iron oxide. One tiny prill of metallic iron observed. |
|---|---|---|---|---|---|---|---|---|---|---|
| 80 | 8007 | Classical/ Hellenistic | TS | None | XX | XX | (see description) | — | — | Fayalite and iron metal-rich slag. Abundant foils of iron metal may replicate original ore morphologies. |
| 80 | 8009 | Classical/ Hellenistic | FS | None | XX | XX | XX | — | — | Significant metallic iron with a variety of morphologies, often corroded. Relict ore morphologies present in iron oxides (corroded metallic iron?) intergrown with silicates. Fayalite and hercynite present as freshly formed phases, but most iron oxides appear to be corroded metallic iron aggregates. |
| 80 | 8010 | Classical/ Hellenistic | FS | — | XX | — | X | — | — | Slag with thin iron silicate laths, virtually no free iron oxides, and many small, rounded prills of metallic iron. At least one large partially reacted ore-gangue fragment is present, identified by silica |

| | | | | | | | | | | |
|---|---|---|---|---|---|---|---|---|---|---|
| | | | | | | | | | | rich matrix and clusters of metallic iron particles. |
| 83 | 8302 | Classical/ Hellenistic | FS | — | — | — | — | — | — | Thin iron silicate laths in non-crystalline or microcrystalline groundmass. |
| 83 | 8303 | Classical/ Hellenistic | TS | — | XX | — | — | — | — | Glassy slag with numerous small, frequently rounded particles of metallic iron. Virtually no crystalline silicate phases. Very similar to 8305. |
| 83 | 8304 | Classical/ Hellenistic | I | — | XX | — | XX | | | Glassy slag with prills of metallic iron. Iron prills are dispersed within a more silica-enriched matrix in a texture suggesting it is a relict ore-gangue fragment where the iron has been reduced and liquified, and the silica has been partially melted. Iron oxides virtually absent. |
| 83 | 8305 | Classical/ Hellenistic | I | — | XX | — | — | — | — | Glassy slag with numerous small, frequently rounded particles of metallic iron. Virtually no crystalline |

| | | | | | | | | | | |
|---|---|---|---|---|---|---|---|---|---|---|
| | | | | | | | | | | silicate phases. Very similar to 8303. |
| 83 | 8306 | Classical/ Hellenistic | FS | Wüstite | XX | XX | — | XX | — | Wüstite and fayalite present in significant quantities. Numerous small particles of metallic iron. Iron sulphides and leucite were also observed. Iron sulphide phases are definitely present. |
| 83 | 8307 | Classical/ Hellenistic | FS | — | X | — | — | — | — | Thin iron silicate laths in non-crystalline or microcrystalline groundmass. A few small particles/prills of metallic iron. |
| 83 | 8308 | Classical/ Hellenistic | I | — | — | XX | — | — | — | Fayalite-dominated slag with piece of minimally-reacted technical ceramic. Al-rich spinels visible near technical ceramic. |
| 84 | 8401 | Medieval | FS/S HB | Wüstite | XX | XX | — | — | — | Wüstite- and fayalite-dominated slag containing small particles of metallic iron throughout. Somewhat corroded. Abundant Al-rich spinels. |

| 84 | 8402 | Medieval | FS/SHB | Wüstite | XX | XX | — | — | — | Wüstite-dominated slag with fayalite, also containing small particles of metallic iron throughout. Somewhat corroded. |
|---|---|---|---|---|---|---|---|---|---|---|
| 84 | 8403 | Medieval | TS | — | X | X | — | — | — | Fayalite-dominated slag with a few small prills of iron. Tapping band. |

The morphology and microstructure of the metallic iron phases is an important indicator of the technological process. Typical bloomery smelting slags, particularly furnace slags, often contain aggregates of metallic iron—metal that did not coalesce with the larger bloom. By contrast slags associated with liquid iron technologies (blast furnace or crucible steel slags, for instance) will often trap small prills of iron. Etched microstructures of metallic iron particles within the slags can reveal compositional information and provide further indications of whether the metal cooled in solid or liquid state. In the heterogeneous environment of the pre-modern smelting furnace, the composition of small particles of metallic iron are not necessarily the same as the overall composition of the iron produced, but they can serve as general indicators of the type of metal produced (see Erb-Satullo *et al.* 2015: 268).

While much of the metallic iron identified in the slags is typical of metallic iron found bloomery smelting slags (spongy aggregates and foils), several samples displayed unusual microstructures. A fragment of reduced ore with dozens of small round prills of iron that failed to fully homogenize with the slag melt was identified in Sample 8304 (of Classical/Hellenistic date) (Figure S5). Rounded particles of iron can form even in a solid state process, but the nearly perfect spherical character of some prills (Figure S5 C) suggests at least some of them were molten. Upon etching, however, most seemed to be predominantly phosphorus-bearing ferrite, while others had a mixture of ferrite and pearlite and one was entirely pearlite. Evidence of spheroidisation was visible in the pearlite structures, indicating a slow cooling process. Another prill also contained a net-like structure of steadite, indicating high phosphorus content and cooling from a liquid state.
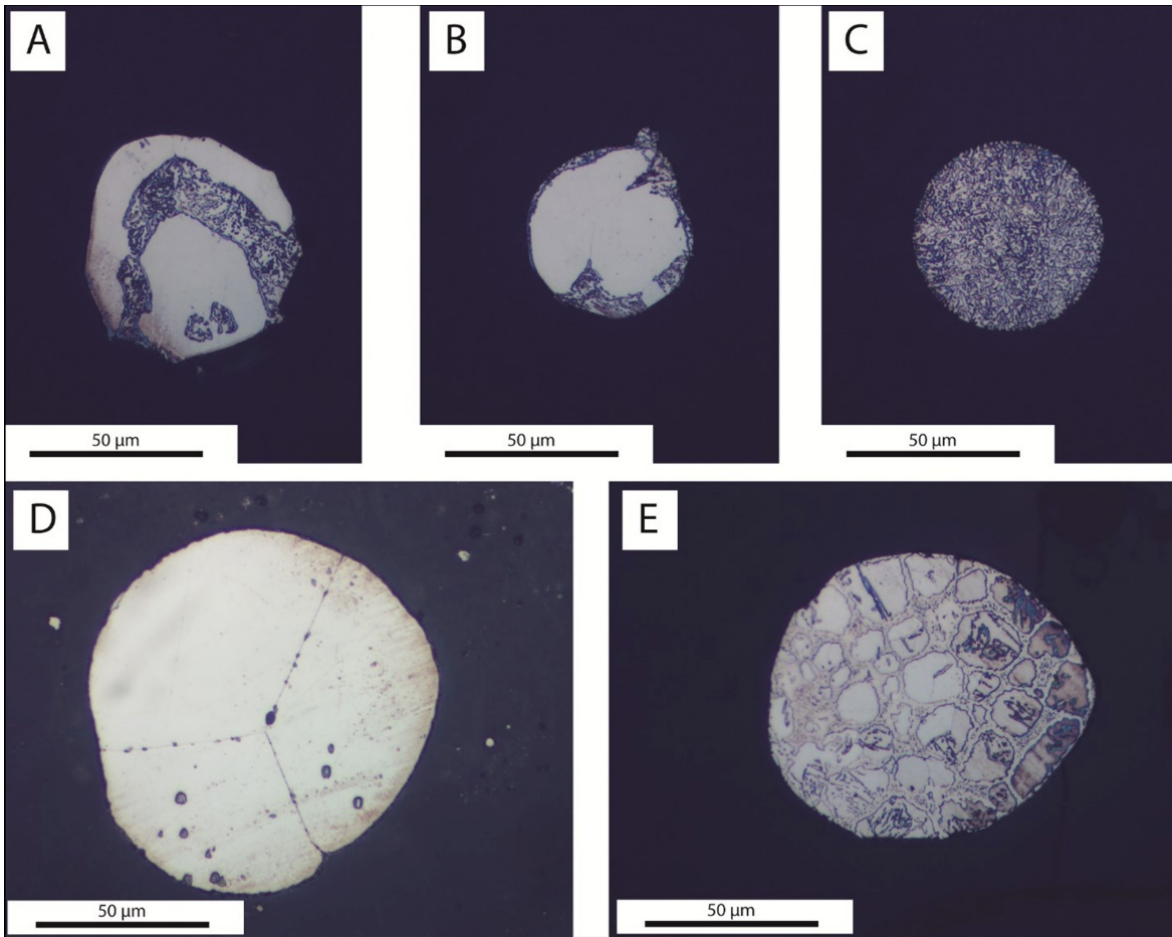
*Figure S5. Optical photomicrographs (PPL) of round iron prills in 8304. A, B – ferrite and pearlite with some spheroidisation; C – pearlite (spheroidised); D – large grained phosphoric ferrite; E – ferrite, (spheroidised) pearlite, and steadite eutectic.*

The metallic aggregate in sample 5906 (of medieval date) also displays a complex microstructure with significant carbon and phosphorus content, which varied considerably across the sample (Figures 9 & S6). In some areas, rounded colonies of pearlite arranged in lines approximates a thick dendritic structure (Figure S6 C), with a well-developed eutectic interspersed between them. In one area, the carbon content was so high enough to induce the formation of cementite laths with pearlite and a eutectic containing both carbon and phosphorus (Figure S6B). This microstructure is a product of the ternary Fe-C-P phase diagram, and the eutectic cannot be adequately explained as either steadite (the eutectic structure of the Fe-P system consisting of ferrite and iron phosphide) or ledeburite (the eutectic structure of the Fe-C system consisting of austenite and cementite, which converts to pearlite and cementite as the metal cools further).

This eutectic consists of a phosphide phase, but it is clear that at least some of the small blebs within it are pearlite rather than ferrite. The laths of cementite present in the sample in between the pearlite colonies indicate a high carbon content and are reminiscent of white cast iron with a composition of over ~2 wt.% C, but in this case, the significant presence of phosphorus complicates precise estimates of the carbon content. Other areas of the sample have lower quantities of phosphorus and carbon, with no eutectic structures. As a whole, these microstructure can be interpreted as evidence of localised melting induced by high carbon and phosphorus content. Some caution is warranted, however, when discussing composition of the overall metal product of these furnaces. While, the iron metal probably contained both carbon and phosphorus, it is difficult to extrapolate quantitative data from this small aggregate. The ~10mm diameter aggregate in 5906 was the largest piece of metal identified in any of the slags, but spongy metallic aggregates, consisting largely of ferrite, were identified in other samples. Even more caution in inferring the composition of the overall product is warranted with the round prills from sample 8304, which are even smaller. More research is necessary, both on finished products and on metal in slags, to narrow down compositional estimates for the typical type of metal produced at these sites.
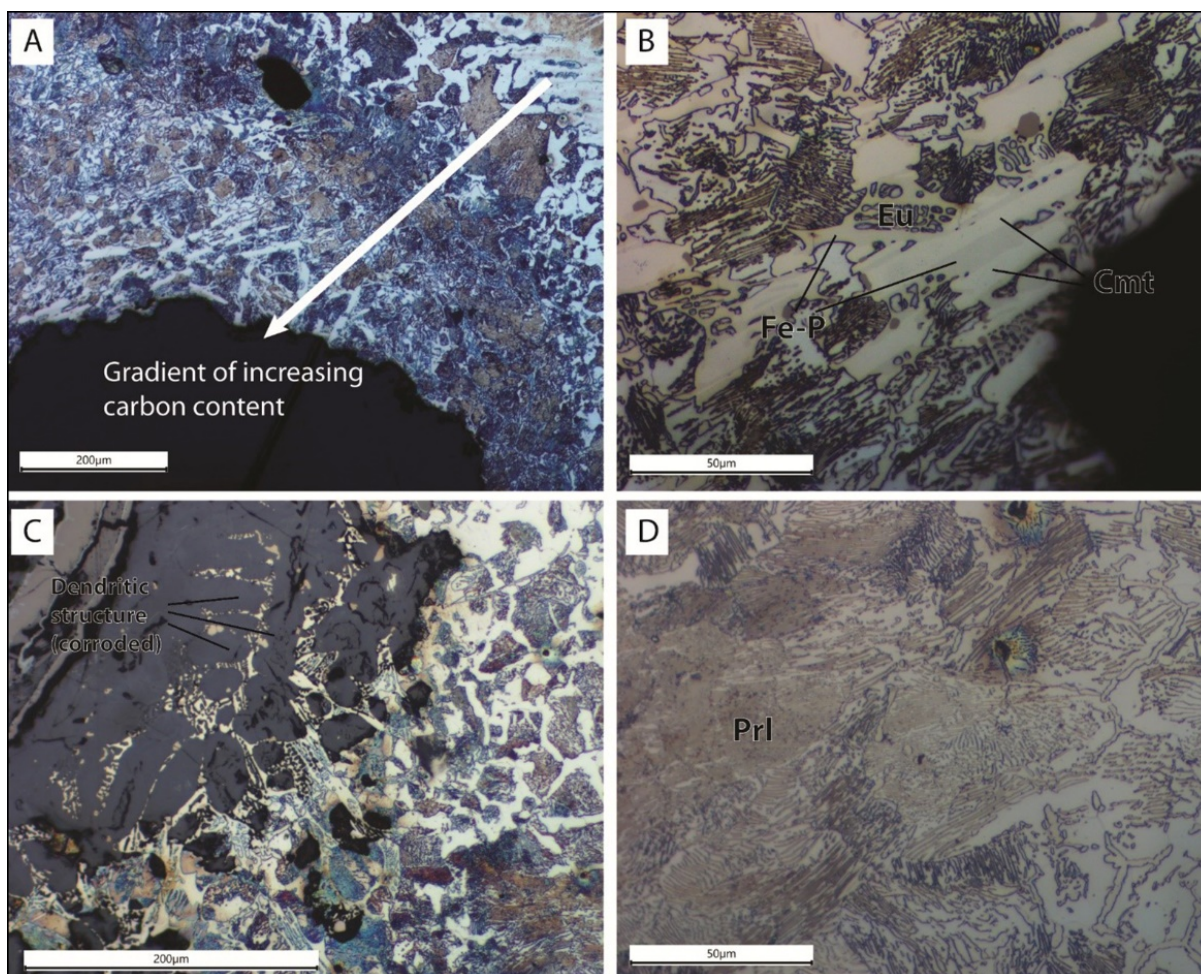
*Figure S6. Additional optical photomicrographs of metal aggregate in Sample 5906 etched with Nital, showing variable carbon and phosphorus content throughout the sample. Abbreviations: Fe-P – iron phosphide, Eu – ternary Fe-C-P eutectic structure, which includes iron phosphide as a constituent phase, Cmt – Cementite.*

SEM-EDS chemical analysis of slags complements microscopic and mineralogical analysis, providing further details about the technological process (Table S4). Areas analyses were conducted on at least four areas and averaged together. Corroded areas, unmelted inclusions, and gas bubbles were avoided wherever possible. For slags containing very large aggregates of metallic iron, two different sets of analyses were taken. One, avoiding the metallic iron aggregates, was intended to characterize the composition of the molten portion of the slag. The other, which included areas with metallic iron aggregates, was intended to approximate the overall composition of both the slag and metal.

**Table S4. Normalised SEM-EDS area analyses of slag. The abbreviation "bdl" indicated "below detection limit" which was conservatively estimated through empirical observation of spectra at 0.2 or 0.3 wt.%.**

| Site # | Sample # | Na$_2$O | MgO | Al$_2$O$_3$ | SiO$_2$ | P$_2$O$_5$ | SO$_2$ | K$_2$O | CaO | TiO$_2$ | MnO | FeO | CuO | ZnO | BaO |
|---|---|---|---|---|---|---|---|---|---|---|---|---|---|---|---|
| 57 | 5701 | 0.8 | 1.8 | 14.2 | 28.2 | 1.6 | 0.3 | 1.4 | 2.3 | 0.6 | bdl | 48.8 | bdl | bdl | bdl |
| 57 | 5702 | 0.8 | 1.6 | 16.1 | 35.3 | 1.3 | bdl | 1.9 | 4.4 | 0.7 | bdl | 37.9 | bdl | bdl | bdl |
| 58 | 5801 | 0.5 | 1.1 | 8.1 | 19.4 | 1.6 | 0.4 | 1.6 | 2.3 | bdl | bdl | 65.0 | bdl | bdl | bdl |
| 58 | 5802 | 0.8 | 1.1 | 9.5 | 25.8 | 1.1 | 0.5 | 1.6 | 3.8 | 0.5 | bdl | 55.2 | bdl | bdl | bdl |
| 59 | 5901 | 0.4 | 0.6 | 7.4 | 17.9 | 0.4 | 0.7 | 1.1 | 2.1 | bdl | bdl | 69.5 | bdl | bdl | bdl |
| 59 | 5902 | 0.5 | 1.0 | 10.8 | 30.3 | 1.1 | 0.5 | 3.1 | 5.0 | 0.6 | bdl | 47.1 | bdl | bdl | bdl |
| 59 | 5903 | 1.9 | 1.4 | 17.2 | 43.0 | 1.3 | 0.7 | 2.3 | 5.3 | 0.9 | bdl | 26.1 | bdl | bdl | bdl |
| 59 | 5904 (no metal) | 1.1 | 3.4 | 13.9 | 41.0 | 1.9 | 0.7 | 5.7 | 11.6 | 0.7 | 0.3 | 19.6 | bdl | bdl | bdl |
| 59 | 5904 (incl. metal) | 0.9 | 4.3 | 11.1 | 31.2 | 2.0 | 0.5 | 3.6 | 11.0 | 0.5 | 0.3 | 34.5 | bdl | bdl | bdl |
| 59 | 5906 | 1.7 | 3.0 | 17.9 | 48.7 | 0.8 | bdl | 3.4 | 8.6 | 1.0 | 0.3 | 14.6 | bdl | bdl | bdl |
| 59 | 5907 | 0.9 | 1.1 | 14.8 | 34.1 | 1.0 | 0.5 | 2.7 | 5.0 | 0.5 | bdl | 39.6 | bdl | bdl | bdl |
| 59 | 5910 | 1.0 | 1.5 | 13.3 | 39.9 | 1.2 | 0.4 | 2.9 | 6.0 | 0.8 | bdl | 33.0 | bdl | bdl | bdl |
| 59 | 5911 | 0.5 | 1.1 | 13.1 | 36.9 | 0.6 | 0.3 | 2.8 | 3.2 | 0.7 | bdl | 40.9 | bdl | bdl | bdl |
| 59 | 5912 (no metal) | 1.6 | 1.7 | 15.8 | 44.4 | 1.1 | 0.6 | 2.6 | 6.8 | 0.9 | bdl | 24.3 | bdl | bdl | bdl |
| 59 | 5912 (incl. metal) | 1.3 | 1.5 | 13.5 | 37.0 | 0.8 | 0.4 | 2.4 | 4.6 | 0.7 | bdl | 37.7 | bdl | bdl | bdl |

| | | | | | | | | | | | | | | |
|---|---|---|---|---|---|---|---|---|---|---|---|---|---|---|
| 59 | 5913 | 0.7 | 0.9 | 10.2 | 34.0 | 0.8 | 0.3 | 2.3 | 3.7 | 0.6 | bdl | 46.6 | bdl | bdl | bdl |
| 59 | 5914 | 0.7 | 1.1 | 10.6 | 35.4 | 0.7 | 0.4 | 2.1 | 5.9 | 0.7 | bdl | 42.5 | bdl | bdl | bdl |
| 66 | 6603 (no metal) | 1.2 | 1.7 | 15.6 | 41.5 | 2.3 | 1.1 | 4.6 | 5.8 | 0.7 | 0.2 | 25.3 | bdl | bdl | bdl |
| 66 | 6603 (incl. metal) | 1.0 | 1.3 | 13.6 | 33.8 | 1.6 | 0.9 | 4.0 | 4.3 | 0.6 | bdl | 38.9 | bdl | bdl | bdl |
| 66 | 6604 (no metal) | 0.7 | 1.1 | 11.3 | 31.1 | 1.9 | 1.3 | 4.5 | 6.8 | 0.5 | bdl | 40.8 | bdl | bdl | bdl |
| 66 | 6604 (incl. metal) | 0.6 | 1.0 | 9.3 | 23.1 | 1.8 | 1.1 | 2.7 | 5.6 | 0.5 | bdl | 54.3 | bdl | bdl | bdl |
| 66 | 6605 (no metal) | 1.2 | 1.7 | 16.7 | 48.4 | 1.2 | 0.8 | 2.6 | 6.7 | 0.9 | bdl | 19.8 | bdl | bdl | bdl |
| 66 | 6605 (incl. metal) | 1.0 | 1.2 | 13.3 | 34.7 | 1.0 | 1.4 | 1.7 | 4.7 | 0.7 | bdl | 40.5 | bdl | bdl | bdl |
| 66 | 6606 (no metal) | 0.7 | 1.9 | 16.2 | 47.6 | 1.0 | 0.2 | 3.4 | 3.2 | 0.9 | bdl | 24.8 | bdl | bdl | bdl |
| 66 | 6606 (incl. metal) | 0.5 | 1.3 | 10.7 | 28.7 | 1.6 | 0.2 | 1.8 | 1.8 | 0.4 | bdl | 52.9 | bdl | bdl | bdl |
| 66 | 6607 | 0.7 | 0.7 | 9.1 | 21.6 | 1.9 | 0.3 | 1.3 | 2.2 | 0.3 | bdl | 61.9 | bdl | bdl | bdl |
| 66 | 6608 | 0.8 | 0.7 | 10.1 | 28.8 | 0.9 | 0.6 | 2.4 | 2.5 | 0.5 | bdl | 52.7 | bdl | bdl | bdl |
| 66 | 6609 | 1.1 | 1.3 | 12.1 | 34.2 | 0.7 | 1.7 | 1.9 | 2.8 | 0.6 | 0.2 | 43.5 | bdl | bdl | bdl |
| 79 | 7901 | 0.2 | 0.4 | 11.4 | 20.1 | bdl | bdl | 0.4 | 1.0 | 0.5 | bdl | 66.2 | bdl | bdl | bdl |

| 80 | 8004 | bdl | 0.5 | 15.4 | 23.6 | bdl | bdl | 0.4 | 0.2 | 0.5 | 0.3 | 59.1 | bdl | bdl | bdl |
| 80 | 8005 | 0.3 | 0.4 | 11.6 | 33.3 | 0.2 | 0.2 | 0.8 | 0.3 | 0.8 | 0.2 | 51.9 | bdl | bdl | bdl |
| 80 | 8006 | 0.2 | 0.4 | 13.5 | 28.3 | 0.2 | bdl | 0.6 | 0.2 | 0.7 | 0.8 | 55.2 | bdl | bdl | bdl |
| 80 | 8007 | 0.2 | 0.4 | 14.6 | 34.7 | 0.2 | 0.2 | 0.8 | 0.3 | 0.8 | 1.3 | 46.6 | bdl | bdl | bdl |
| 80 | 8009 | 0.2 | 0.5 | 17.1 | 43.9 | bdl | 0.2 | 0.9 | 0.3 | 0.9 | 2.8 | 33.2 | bdl | bdl | bdl |
| 83 | 8302 | 1.1 | 1.4 | 13.3 | 43.5 | 0.8 | 0.3 | 1.8 | 2.8 | 0.6 | 1.7 | 32.6 | bdl | bdl | bdl |
| 83 | 8303 | 0.9 | 2.6 | 11.9 | 44.6 | 0.7 | 0.4 | 1.6 | 3.5 | 0.6 | 1.3 | 31.8 | bdl | bdl | bdl |
| 83 | 8304 | bdl | 0.8 | 17.8 | 41.0 | 0.7 | bdl | 0.8 | 0.7 | 1.0 | 1.8 | 35.1 | bdl | bdl | 0.3 |
| 83 | 8305 | 1.0 | 1.5 | 14.0 | 47.3 | 0.5 | bdl | 1.6 | 0.8 | 0.7 | 0.8 | 31.9 | bdl | bdl | bdl |
| 83 | 8306 | 0.2 | 0.9 | 10.3 | 20.8 | 0.2 | 0.6 | 0.4 | 0.5 | 0.3 | 0.4 | 65.4 | bdl | bdl | bdl |
| 83 | 8307 | 0.6 | 0.8 | 16.1 | 41.0 | 0.6 | bdl | 1.5 | 0.5 | 0.8 | 0.7 | 37.4 | bdl | bdl | bdl |
| 83 | 8308 | 0.8 | 1.1 | 16.3 | 44.0 | 0.6 | bdl | 1.4 | 1.2 | 0.7 | 0.7 | 33.2 | bdl | bdl | bdl |
| 84 | 8401 | 0.2 | 0.7 | 11.5 | 21.9 | 0.2 | 0.2 | 1.0 | 0.8 | 0.4 | 0.3 | 62.9 | bdl | bdl | bdl |
| 84 | 8402 | 0.4 | 0.6 | 7.0 | 21.4 | 0.4 | bdl | 1.2 | 3.4 | 0.3 | bdl | 65.4 | bdl | bdl | bdl |
| 84 | 8403 | 0.3 | 0.6 | 12.5 | 29.9 | bdl | bdl | 1.1 | 1.1 | 0.5 | 0.7 | 53.2 | bdl | bdl | bdl |

Instead of binary plots, it is often useful to plot slag chemistry on a ternary phase diagram to understand the behaviour of the melt (Figure S7). Such plots are very much approximations, as they ignore other elements that are present in the slags, and most phase diagrams are based on equilibrium conditions, which do not occur in ancient smelting furnaces. Nonetheless, because slag chemistry, especially the relative proportions of iron and silicon, is correlated with the redox conditions in the furnace and the carbon content of the metallic product (Tylecote *et al.* 1971; Rehder 2000: 125–26; Rehren *et al.* 2007), such plots can be useful. Two phase diagrams commonly used to plot iron slag data were used, the $SiO_2$-$FeO$-$Al_2O_3$ diagram for low-calcium slags and the $SiO_2$-$FeO$-Anorthite ($CaAl_2Si_2O_8$) diagram for higher calcium slags (Morton & Wingrove 1972, 1969; Rehren *et al.* 2007; Charlton *et al.* 2010). MnO content was added to FeO content for the purposes of the phase diagram, given their similar behaviour in slag melts. Compositions were converted to anorthite from the oxide wt.% values by calculating the maximum wt.% of anorthite that could form given the existing calcium, aluminium, and silicon content of the slag. For each sample, the preferred ternary phase diagram for display was chosen based on which ternary sum account for a greater proportion of the actual composition (in most cases 85–95 per cent of the total EDS normalised composition). For each sample, in order to plot them on a ternary diagram, values for the chosen three components were normalised to that they added to 100 per cent.
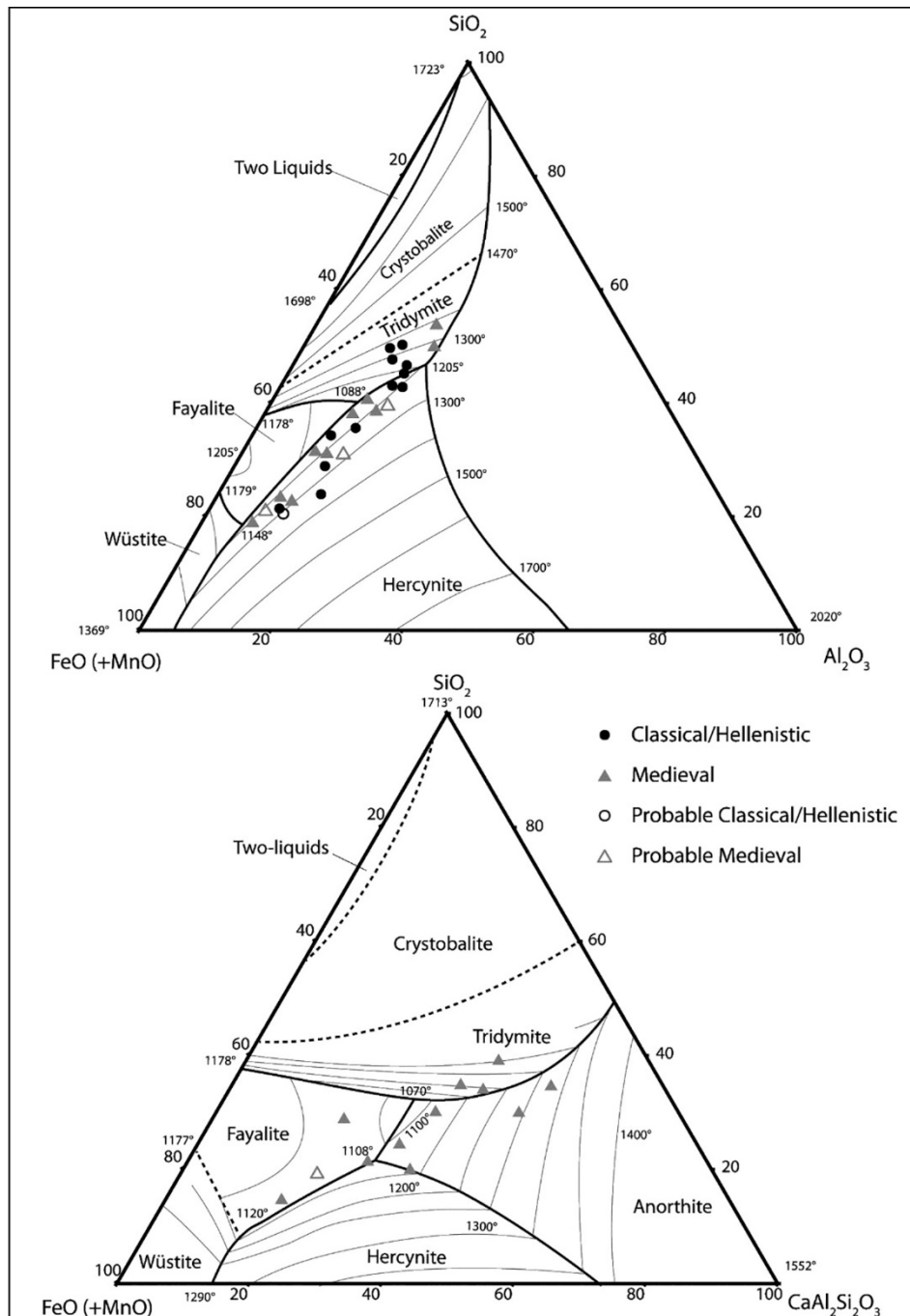
*Figure S7. Plots of slag chemistries as measured by SEM-EDS on ternary phase diagrams. For samples with large aggregates of solid metallic iron, only analyses avoiding these aggregates are plotted. Note that melting temperatures and the phases indicated on the diagram represent an idealized ternary system at equilibrium.*

Ternary plots of slag chemistries reveal that a substantial number cluster around the low-iron eutectic in the $SiO_2$-$FeO$-$Al_2O_3$ phase diagram, a slag composition that is typically correlated with higher reducing conditions in the furnace, higher carbon content in the resulting iron, and higher fuel to ore ratios in the furnace charge (Charlton *et al.* 2010: 356–57). These results are consistent with the identification of mostly or completely vitreous slags, the prevalence of metallic iron over iron oxides, and metallographic evidence suggesting the production of some liquid iron in these furnaces. Since slags are not formed in equilibrium conditions and contain other elements, slag melting temperatures would have differed from those indicated on the diagram, and some of the phases indicated on the diagrams do not typically form in slags.

The composition of the ore fragments was also measured by SEM-EDS area analyses (Table S5), but one should keep in mind that this does not include the weight of any lighter elements (e.g. hydrogen) bound up in iron hydroxides. Moreover, some of the ore samples (e.g. 6611) were extremely heterogeneous, with some areas higher in quartz, and others higher in iron oxides. As a result, these values should be interpreted more qualitatively than quantitatively.

The compositions of five glassy slags (5910, 5911, 6606, 8303, 8304, 8305) were also measured by wavelength-dispersive electron microprobe at the Research Lab for Archaeology and the History of Art at Oxford (Table S6). Several spots on each sample were measured, avoiding any non-molten inclusions. Agreement with EDS area analyses was good.

**Table S5. Normalised SEM-EDS area analyses of ores. Note that iron ores may contain significant hydroxides and other light elements which are not detected by SEM-EDS. The abbreviation "bdl" indicated "below detection limit" which was conservatively estimated through empirical observation of spectra at 0.2 or 0.3 wt.%.**

| Site # | Sample # | Na$_2$O | MgO | Al$_2$O$_3$ | SiO$_2$ | P$_2$O$_5$ | SO$_2$ | K$_2$O | CaO | TiO$_2$ | MnO | FeO | CuO | ZnO | BaO |
|--------|----------|---------|-----|-------------|---------|------------|--------|--------|-----|---------|-----|------|-----|-----|-----|
| 59 | 5905 | bdl | bdl | 2.4 | 20.1 | bdl | 0.3 | bdl | bdl | 0.4 | bdl | 76.9 | bdl | bdl | bdl |
| 59 | 5908 | bdl | 0.3 | 2.6 | 6.0 | bdl | 0.6 | bdl | bdl | bdl | bdl | 90.5 | bdl | bdl | bdl |
| 59 | 5909 | bdl | bdl | 4.9 | 31.2 | 0.3 | 0.3 | 0.3 | bdl | 0.6 | bdl | 62.4 | bdl | bdl | bdl |
| 66 | 6601 | bdl | bdl | 0.6 | 23.5 | 0.3 | 0.3 | bdl | 0.2 | 1.1 | bdl | 74.0 | bdl | bdl | bdl |
| 66 | 6610 | 0.4 | 0.2 | 7.7 | 43.7 | 0.5 | 2.7 | 0.9 | 0.3 | 0.8 | bdl | 42.9 | bdl | bdl | bdl |
| 66 | 6611 | 0.7 | 0.6 | 13.5 | 41.1 | 0.5 | 0.6 | 1.8 | 0.3 | 0.9 | bdl | 40.0 | bdl | bdl | bdl |
| 66 | 6612 | 0.3 | 0.4 | 11.9 | 41.7 | 0.7 | 0.2 | 1.9 | 0.3 | 0.7 | bdl | 42.0 | bdl | bdl | bdl |
| 83 | 8301 | bdl | bdl | 5.9 | 25.6 | bdl | bdl | 0.2 | bdl | 0.4 | 0.3 | 67.6 | bdl | bdl | bdl |

**Table S6. WDS microprobe spot analyses of vitreous slags (wt.%). Data were normalised, but the non-normalised analytical totals are reported as well. Multiple spots were analysed on each sample. Limits of quantification (bdl) vary between 0.06 and 0.19 for different elements.**

| Site # | Sample # | Spot # | Na$_2$O | MgO | Al$_2$O$_3$ | SiO$_2$ | P$_2$O$_5$ | SO$_2$ | K$_2$O | CaO | TiO$_2$ | MnO | FeO | CuO | Total |
|---|---|---|---|---|---|---|---|---|---|---|---|---|---|---|---|
| 59 | 5910 | 1 | 1.06 | 1.60 | 12.85 | 40.87 | 1.18 | 0.14 | 2.94 | 6.71 | 0.85 | bdl | 31.80 | bdl | 93.29 |
| 59 | 5910 | 2 | 1.17 | 1.76 | 14.05 | 42.35 | 1.24 | 0.15 | 3.04 | 6.50 | 0.75 | bdl | 28.99 | bdl | 95.95 |
| 59 | 5910 | 3 | 1.13 | 1.92 | 13.39 | 41.54 | 1.28 | 0.10 | 3.03 | 5.62 | 0.84 | bdl | 31.14 | bdl | 95.23 |
| 59 | 5910 | 4 | 1.09 | 1.74 | 13.29 | 41.89 | 1.24 | 0.13 | 3.06 | 6.72 | 0.75 | bdl | 29.94 | 0.15 | 95.64 |
| 59 | 5910 | 5 | 1.09 | 1.61 | 13.20 | 42.15 | 1.22 | 0.13 | 2.75 | 6.90 | 0.90 | 0.19 | 29.84 | bdl | 93.59 |
| 59 | 5910 | 6 | 1.18 | 1.85 | 13.16 | 42.30 | 1.18 | 0.13 | 2.85 | 6.76 | 0.80 | bdl | 29.78 | bdl | 95.45 |
| 59 | 5911 | 1 | 0.48 | 1.05 | 13.31 | 39.28 | 0.64 | 0.10 | 2.86 | 3.44 | 0.81 | bdl | 38.03 | bdl | 96.72 |
| 59 | 5911 | 2 | 0.40 | 1.02 | 13.19 | 39.06 | 0.68 | 0.10 | 2.94 | 3.34 | 0.80 | bdl | 38.47 | bdl | 96.09 |
| 59 | 5911 | 3 | 0.51 | 1.04 | 13.38 | 39.89 | 0.72 | 0.11 | 3.02 | 3.53 | 0.84 | bdl | 36.98 | bdl | 96.04 |
| 59 | 5911 | 4 | 0.55 | 1.00 | 13.29 | 39.59 | 0.66 | 0.09 | 2.95 | 3.48 | 0.81 | bdl | 37.57 | bdl | 95.32 |
| 59 | 5911 | 5 | 0.43 | 0.94 | 13.05 | 39.35 | 0.64 | 0.11 | 2.90 | 3.21 | 0.82 | bdl | 38.55 | bdl | 96.26 |
| 59 | 5911 | 6 | 0.39 | 0.99 | 13.05 | 38.79 | 0.70 | 0.10 | 2.79 | 3.35 | 0.73 | bdl | 39.11 | bdl | 96.48 |
| 66 | 6606 | 1 | 0.82 | 1.81 | 17.53 | 52.28 | 0.71 | bdl | 4.18 | 3.34 | 0.94 | bdl | 18.39 | bdl | 97.18 |
| 66 | 6606 | 2 | 0.76 | 1.94 | 17.59 | 51.10 | 0.74 | bdl | 3.71 | 3.40 | 0.98 | bdl | 19.77 | bdl | 96.59 |
| 66 | 6606 | 3 | 0.92 | 1.88 | 17.87 | 51.60 | 0.84 | 0.07 | 4.01 | 3.34 | 0.95 | bdl | 18.51 | bdl | 97.15 |
| 66 | 6606 | 4 | 0.64 | 1.97 | 18.19 | 50.89 | 0.86 | bdl | 3.91 | 4.02 | 0.95 | bdl | 18.58 | bdl | 96.71 |
| 66 | 6606 | 5 | 0.85 | 1.97 | 18.47 | 52.71 | 0.83 | bdl | 4.01 | 3.45 | 1.02 | bdl | 16.67 | bdl | 97.10 |

| 83 | 8303 | 1 | 0.69 | 2.44 | 12.22 | 46.56 | 0.66 | 0.15 | 1.72 | 3.55 | 0.68 | 1.42 | 29.90 | bdl | 95.99 |
|----|------|---|------|------|-------|-------|------|------|------|------|------|------|-------|-----|-------|
| 83 | 8303 | 2 | 0.85 | 2.48 | 11.92 | 47.10 | 0.64 | 0.13 | 1.77 | 3.53 | 0.68 | 1.46 | 29.45 | bdl | 95.33 |
| 83 | 8303 | 3 | 0.55 | 2.62 | 11.33 | 43.82 | 0.74 | 0.15 | 1.30 | 3.60 | 0.71 | 1.47 | 33.72 | bdl | 96.01 |
| 83 | 8303 | 4 | 0.76 | 2.47 | 11.89 | 46.18 | 0.68 | 0.14 | 1.69 | 3.60 | 0.69 | 1.52 | 30.37 | bdl | 95.91 |
| 83 | 8303 | 5 | 0.73 | 2.49 | 12.34 | 48.41 | 0.60 | 0.14 | 1.87 | 3.62 | 0.64 | 1.37 | 27.79 | bdl | 96.40 |
| 83 | 8303 | 6 | 0.93 | 2.45 | 12.01 | 46.52 | 0.69 | 0.14 | 1.75 | 3.58 | 0.68 | 1.36 | 29.89 | bdl | 95.46 |
| 83 | 8304 | 1 | bdl | 0.73 | 17.88 | 42.36 | 0.63 | bdl | 0.96 | 0.77 | 1.05 | 1.97 | 33.66 | bdl | 95.67 |
| 83 | 8304 | 2 | bdl | 0.79 | 18.27 | 42.40 | 0.63 | bdl | 0.98 | 0.76 | 1.09 | 1.89 | 33.19 | bdl | 94.23 |
| 83 | 8304 | 3 | bdl | 0.74 | 17.76 | 41.97 | 0.71 | bdl | 0.92 | 0.62 | 1.05 | 1.79 | 34.43 | bdl | 94.79 |
| 83 | 8304 | 4 | bdl | 0.72 | 17.76 | 41.28 | 0.71 | bdl | 0.81 | 0.66 | 1.07 | 1.82 | 35.17 | bdl | 94.98 |
| 83 | 8304 | 5 | bdl | 0.80 | 18.13 | 42.60 | 0.68 | bdl | 1.00 | 0.75 | 1.07 | 1.81 | 33.17 | bdl | 95.28 |
| 83 | 8304 | 6 | bdl | 0.74 | 17.99 | 41.98 | 0.71 | bdl | 0.84 | 0.62 | 1.06 | 1.83 | 34.22 | bdl | 94.51 |
| 83 | 8305 | 1 | 1.02 | 1.26 | 14.50 | 49.60 | 0.47 | bdl | 1.64 | 0.80 | 0.82 | 0.90 | 28.98 | bdl | 96.18 |
| 83 | 8305 | 2 | 0.82 | 1.29 | 14.18 | 49.55 | 0.48 | bdl | 1.59 | 0.78 | 0.76 | 0.72 | 29.83 | bdl | 95.82 |
| 83 | 8305 | 3 | 0.80 | 1.34 | 14.17 | 49.53 | 0.49 | bdl | 1.60 | 0.79 | 0.78 | 0.88 | 29.61 | bdl | 96.81 |
| 83 | 8305 | 4 | 0.94 | 1.39 | 14.02 | 49.32 | 0.43 | bdl | 1.61 | 0.85 | 0.79 | 0.88 | 29.78 | bdl | 95.83 |
| 83 | 8305 | 5 | 0.78 | 1.35 | 14.01 | 49.10 | 0.53 | bdl | 1.62 | 0.80 | 0.73 | 0.87 | 30.21 | bdl | 95.91 |
| 83 | 8305 | 6 | 0.98 | 1.39 | 14.17 | 49.18 | 0.46 | bdl | 1.68 | 0.83 | 0.74 | 0.80 | 29.79 | bdl | 96.76 |

**References**

BRONK RAMSEY, C. 2013. OxCal v.4.2.4. Available at: https://c14.arch.ox.ac.uk/oxcal.html (accessed 29 january 2020).

CHARLTON, M.F., P. CREW, T. REHREN & S.J. SHENNAN. 2010. Explaining the evolution of ironmaking recipes: an example from north-west Wales. *Journal of Anthropological Archaeology* 29: 352–67. https://doi.org/10.1016/j.jaa.2010.05.001

ERB-SATULLO, N.L., B.J.J. GILMOUR, & N. KHAKHUTAISHVILI. 2015. Crucible technologies in the Late Bronze–Early Iron Age South Caucasus: copper processing, tin bronze production and the possibility of local tin ores. *Journal of Archaeological Science* 61: 260–76. https://doi.org/10.1016/j.jas.2015.05.010

– 2017. Copper production landscapes of the South Caucasus. *Journal of Anthropological Archaeology* 47: 109–26. https://doi.org/10.1016/j.jaa.2017.03.003

– 2018. The ebb and flow of copper and iron smelting in the South Caucasus. *Radiocarbon* 60: 159–80. https://doi.org/10.1017/RDC.2017.87

KHAKHUTAISHVILI, D.A. 2009. *The manufacture of iron in ancient Colchis* (British Archaeological Reports International Series 1905). Oxford: Archaeopress.

MORTON, G.R. & J. WINGROVE. 1969. Constitution of bloomery slags: part I: Roman. *Journal of the Iron and Steel Institute* 207: 1556–64.

– 1972. Constitution of bloomery slags: part II: medieval. *Journal of the Iron and Steel Institute* 210: 478–88.

MURALHA, V.S.F., T. REHREN & R.J.H. CLARK. 2011. Characterisation of an iron smelting slag from Zimbabwe by Raman microscopy and electron beam analysis. *Journal of Raman Spectroscopy* 42: 2077–84. https://doi.org/10.1002/jrs.2961

REIMER, P.J. *et al*. 2013. IntCal13 and Marine13 radiocarbon age calibration curves 0–50 000 years cal BP. *Radiocarbon* 55: 1869–87. https://doi.org/10.2458/azu_js_rc.55.16947

REHDER, J.E. 2000. *Mastery and uses of fire in antiquity*. Montreal & Kingston: McGill-Queen's University Press.

REHREN, T., M. CHARLTON, S. CHIRIKURE, J. HUMPHRIS, A. IGE & H.A. VELDHUIZJEN. 2007. Decisions set in slag: the human factor in African iron smelting, in S. LaNiece, D. Hook & P. Craddock (ed.) *Metals and Mine: Studies in Archaeometallurgy*: 211–18. London: Archetype.

TYLECOTE, R.F., J.M. AUSTIN & A.E. WRAITH. 1971. The mechanism of the bloomery process in the shaft furnaces. *Journal of the Iron and Steel Institute* 209: 243–63.